

SCIENTIFIC REPORTS

OPEN

Photoelectron Holographic Atomic Arrangement Imaging of Cleaved Bimetal-intercalated Graphite Superconductor Surface

Fumihiko Matsui¹, Ritsuko Eguchi², Saki Nishiyama², Masanari Izumi², Eri Uesugi², Hidenori Goto², Tomohiro Matsushita³, Kenji Sugita¹, Hiroshi Daimon¹, Yuji Hamamoto⁴, Ikutaro Hamada⁵, Yoshitada Morikawa⁴ & Yoshihiro Kubozono^{2,6}

Received: 04 April 2016
Accepted: 11 October 2016
Published: 04 November 2016

From the C 1s and K 2p photoelectron holograms, we directly reconstructed atomic images of the cleaved surface of a bimetal-intercalated graphite superconductor, (Ca, K)C₈, which differed substantially from the expected bulk crystal structure based on x-ray diffraction (XRD) measurements. Graphene atomic images were collected in the in-plane cross sections of the layers 3.3 Å and 5.7 Å above the photoelectron emitter C atom and the stacking structures were determined as AB- and AA-type, respectively. The intercalant metal atom layer was found between two AA-stacked graphenes. The K atomic image revealing 2 × 2 periodicity, occupying every second centre site of C hexagonal columns, was reconstructed, and the Ca 2p peak intensity in the photoelectron spectra of (Ca, K)C₈ from the cleaved surface was less than a few hundredths of the K 2p peak intensity. These observations indicated that cleavage preferentially occurs at the KC₈ layers containing no Ca atoms.

Various graphite intercalation compound (GIC) superconductors have been developed using liquid-metal-alloy (LMA) and vapour-transport (VT) methods^{1–13}. The highest value of the superconducting transition temperature, T_c , for the GIC superconductors at ambient pressure is currently 11.5 K for CaC₆^{6,7}. The strong electron-phonon coupling between the electronic state at the interlayer Ca atoms and vertical graphite vibration has been regarded as the origin of this high T_c ⁸. Most GIC superconductors have been shown to exhibit increased T_c under applied pressure^{9–12}. By applying pressure up to 7.5 GPa, the T_c of CaC₆ increased to 15.1 K⁹, which is the highest T_c realized for a GIC superconductor. The increase in T_c was attributed to the softening of the Ca-Ca phonon under high pressure¹⁰.

Other than the confirmation of T_c at 65 mK for BaC₆¹³, the members of the GIC superconductor family have remained unchanged for the past nine years. However, we recently successfully fabricated a new series of bimetal-intercalated graphite superconductors, Ca_xK_{1-x}C_y¹⁴. The T_c of Ca_xK_{1-x}C_y continuously increased to 11.5 K ($x = 1$; CaC₆) nonlinearly as x increased. The T_c of KC₈ was only 136 mK, but the introduction of a very small amount of Ca drastically increased this value¹⁴. The bulk crystal structure was assigned as ‘KC₈’ type for x less than 0.7 and as ‘CaC₆’ type for $x = 1$ (Supplementary information Fig.S1). K and Ca atoms form 2 × 2 and ($\sqrt{3} \times \sqrt{3}$) – R30° two-dimensional lattices in KC₈ and CaC₆, respectively. The vertical arrangements of graphene sheets and K atoms are denoted as ‘AαAβAγδ’, where ‘A’ corresponds to the graphene sheet, and α, β, γ, and δ refer to the sites occupied by metal atoms. Moreover, the arrangements of graphene sheets and Ca atoms are denoted as ‘AαAβAγ’⁶. The distance between graphene sheets, d_{AA} , in KC₈ (5.35 Å) is larger than that in CaC₆ (4.524 Å)⁶, suggesting that graphene layers are more strongly bounded by Ca atom intercalation.

¹Graduate School of Materials Science, Nara Institute of Science and Technology, Ikoma, Nara 630-0192, Japan. ²Research Laboratory for Surface Science, Okayama University, Okayama 700-8530, Japan. ³Japan Synchrotron Radiation Research Institute, SPring-8, Sayo, Hyogo 679-5198, Japan. ⁴Graduate School of Engineering, Osaka University, Suita 565-0871, Japan. ⁵International Center for Materials Nanoarchitectonics (WPI-MANA) and Global Research Center for Environmental and Energy based on Nanomaterials Science (GREEN), National Institute for Materials Science (NIMS), 1-1 Namiki Tsukuba 305-0044, Japan. ⁶Research Centre of New Functional Materials for Energy Production, Storage and Transport, Okayama University, Okayama 700-8530, Japan. Correspondence and requests for materials should be addressed to F.M. (email: matui@ms.naist.jp)

It is essential to directly visualize three-dimensional (3D) atomic arrangements around intercalant atoms to understand the superconducting mechanism, but the local structure around the intercalant atoms of bimetal GIC superconductors remains unknown because the methods available for the local structure analysis were previously limited. Recently, a new holography algorithm, scattering pattern-extraction algorithm (SPEA)-maximum entropy method (MEM), has been developed for atomic arrangement reconstruction^{15–18}. Photoelectron holography is based on photoelectron spectroscopy and diffraction and is used for electronic structure, chemical composition, and atomic arrangement analyses^{19–22}. The 3D image of atomic arrangement around the photoelectron emitter atom can be directly obtained from the element-specific holograms^{15–18,22}. Furthermore, the surface phonon is often softened²³ by the bulk truncation, structure modification, and interaction with the substrate. Surface layer²⁴ and monoatomic thin film^{25,26} superconductivity have been realized and have attracted substantial fundamental interest. Because of the short probing depth of photoelectrons, photoelectron holography is one of the most effective methods for studying surface and subsurface atomic structures in 3D. Complementarily, 3D atomic arrangement images of the bulk can be obtained by fluorescent x-ray holography having longer probing depth^{27,28}.

Here, we demonstrate the effectiveness of photoelectron holography in the study of the surface of superconducting materials prepared by intercalation with metal atoms. Below, the sample studied here is represented by '(Ca, K)C₈'. In the present study, we successfully measured photoelectron spectra and holography data for superconducting (Ca, K)C₈, which was recently prepared by our group¹⁴. The photoelectron spectra of the cleaved surface of (Ca, K)C₈ showed only C 1s and K 2p peaks, and the Ca 2p peak intensity was less than a few hundredths of that of the K 2p peak. We directly obtained the images of C and metal atomic arrangements at the (Ca, K)C₈ cleaved surface reconstructed from the C 1s and K 2p photoelectron holograms. The K atoms were found to be located in the centres of the C hexagon columns of the graphene sheets stacked in an AA arrangement. Furthermore, the graphite-layered structure without intercalated metal atoms was confirmed to exhibit an AB arrangement. Thus, the cleaved surface region of GIC was demonstrated to have a stage 2 structure by photoelectron holography, which differed substantially from the expected bulk (Ca, K)C₈ crystal structure elucidated from the x-ray diffraction (XRD) measurements. These observations revealed that the cleavage preferentially occurs at the stage-2 type K atom intercalated layers containing no Ca atoms, which is likely the most fragile part of the crystal sample.

Results

Characterization of (Ca, K)C₈. The (Ca, K)C₈ bimetal GIC lumps were prepared by the LMA technique, in which Ca and K are mixed together with a molar ratio of $x':1-x'$ and excess Li. In the present case, the experimental nominal value x' was 0.7.

The magnetic susceptibility, χ_g (cm³ g⁻¹), of the present (Ca, K)C₈ sample is shown in Fig. 1a; $\chi_g = \frac{MV}{WH}$, where MV (G cm³), W (g) and H (Oe) are the superconducting quantum interference device (SQUID) magnetic moment and weight of the sample and the applied magnetic field, respectively. T_c was determined from the cross points of two extrapolated lines of the χ_g -temperature (T) plot in the normal and rapid drop regions (see Fig. 1a). The single T_c at 9.9 K was observed, and the shielding fraction (2.5 K) was nearly 100%, suggesting homogeneous bimetal intercalation throughout most of the bulk region. Figure 1b shows the plot of T_c versus an experimental nominal value x' for a Ca _{x} K _{$1-x$} C _{y} series based on this study and our previous report¹⁴. T_c increases continuously with increasing x' in Ca _{x} K _{$1-x$} C _{y} , suggesting that the Ca and K atoms were intercalated into graphite according to each equilibrium constant.

The energy-dispersive x-ray (EDX) spectroscopy of the ground (Ca, K)C₈ powder exhibited all peaks of C, K, and Ca atoms shown in Fig. 1c. The EDX showed that the chemical composition was Ca_{0.11(3)}K_{0.89(3)}C_{7.1(4)}. The peak intensity ascribable to Ca atom was quite low compared with the nominal molar ratio ($x' = 0.7$). This suggests that the equilibrium constant for Ca atom intercalation was much smaller than that of K atom intercalation. However, the fact that the (Ca, K)C₈ sample with such a small x value featured $T_c = 10$ K is surprising, as seen in Fig. 1b. This small x value (0.11) may be associated with an overestimation of the K concentration ratio because of metallic K residue and the low Ca concentration ratio at the cleaved surface of (Ca, K)C₈, as suggested from the following photoelectron spectroscopy results.

The out-of-plane XRD pattern (Fig. 1d) of the (Ca, K)C₈ sample showed the same pattern as the simulated result of KC₈. Only 00 l reflections were observed in the XRD pattern, indicating that the present (Ca, K)C₈ sample was highly oriented along the c -axis. The graphene interlayer distance was determined to be 5.38(2) Å, which is nearly equal to one fourth of the lattice constant c , 21.40 Å, of KC₈³ with a face-centred orthorhombic (fco) bulk structure: $Fddd$ (No. 70).

Photoelectron spectroscopy and holography of (Ca, K)C₈. Prior to the photoemission measurement, we cleaved the (Ca, K)C₈ lump under an oxygen-free pure Ar gas environment and then placed it in an ultrahigh vacuum chamber without exposing it to atmosphere. Figure 2a shows the photoelectron spectra of (Ca, K)C₈ and graphite normalized by the C 1s peak intensity at a kinetic energy of 628 eV. As indicated by the difference spectrum, the Ca 2p peak intensity from the cleaved surface was less than a few hundredths of the K 2p peak intensity. Li 1s peak at the binding energy of 56 eV was below the detection limit (not shown). The inelastic mean free path of the photoelectron along the interlayer direction at a kinetic energy of approximately 600 eV was on the order of 2 nm²⁹. Therefore, no Li or Ca atoms were present within the surface region of a few graphite layers. Li atoms seem to have been completely replaced by Ca and K atoms during the sample preparation. These results are consistent with the previous conclusion^{7,8} that Li metal is removed from the graphite after Ca or K intercalation. Because the EDX result indicated the existence of Ca atoms in the bulk, two scenarios can be suggested: (1) Ca was removed from the surface after cleavage of the (Ca, K)C₈ lump and (2) a region without Ca was cleaved. Because the vapour pressures of Ca and Ca compounds are sufficiently low at room temperature, the first scenario is excluded.

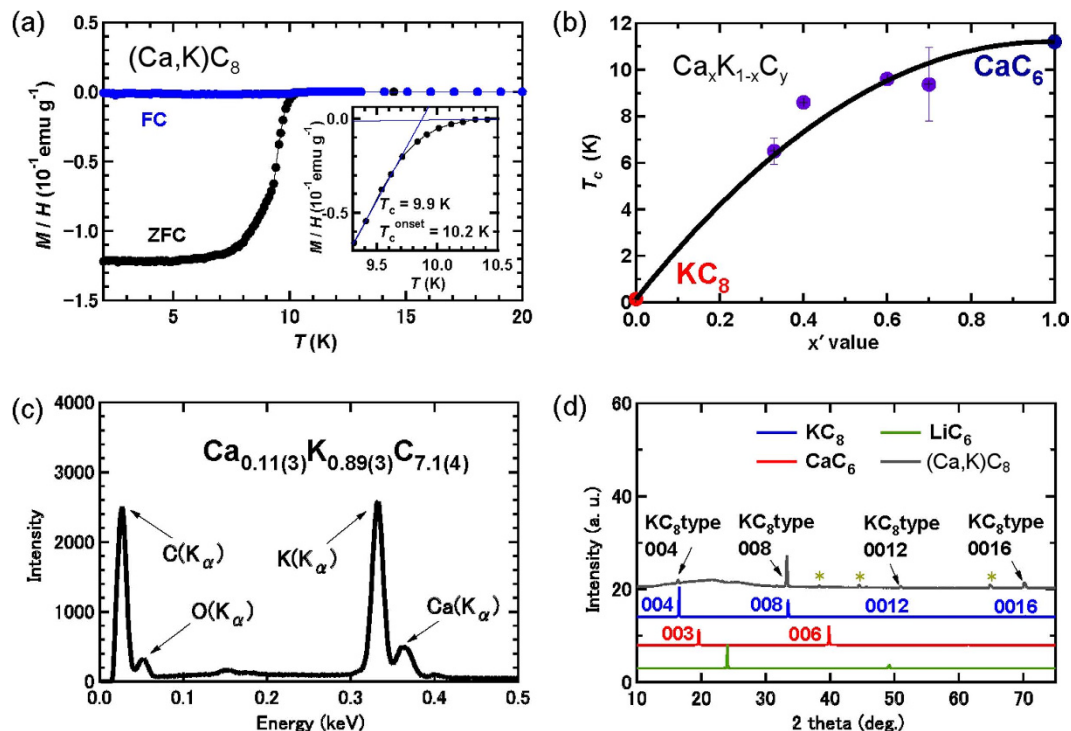


Figure 1. (a) M/H vs. T plots for $(Ca, K)C_8$ (ZFC and FC modes) at ambient pressure. (b) x vs. T_c plots of $Ca_xK_{1-x}C_y$. (c) EDX spectrum of $(Ca, K)C_8$. (d) Experimental XRD pattern of $(Ca, K)C_8$ and simulated patterns for KC_8 , CaC_6 and LiC_6 . The peaks labelled ‘*’ in the experimental XRD pattern can be assigned to the Al of the sample holder. The same sample of $(Ca, K)C_8$ was used to obtain the $M/H - T$ plots shown in 1a and the XRD pattern shown in 1c, whereas the sample used for the EDX spectrum shown in 1d is different; however, the nominal x value and observed T_c are the same.

Because graphene layers are more strongly bounded by Ca than K intercalation, it is reasonable to conclude that cleavage occurs selectively at the layers without Ca atoms.

Full-hemisphere photoelectron holograms were recorded for C 1s and K 2p, as shown in Fig. 2b,c (Supplementary information Fig.S2). The holograms are represented in a stereo projection so that diffraction rings appear as circles²⁹. Yellow-dashed and red-solid arcs in the C 1s hologram correspond to the diffraction rings around the directions along and perpendicular to the shortest CC bonds of graphite, respectively. The diffraction feature resembling the C 1s hologram also appeared as a background in the measured K 2p hologram because of the energy-loss components of C 1s photoelectrons³⁰. The intrinsic C 1s and K 2p holograms (I_C and I_K) shown in Fig. 2b,c, respectively, were obtained by solving a simultaneous equation (Supplementary information Fig.S3). The raw C 1s and K 2p holograms consisted of $0.95I_C + 0.05I_K$ and $0.475I_C + 0.525I_K$, respectively. The coefficients were determined by considering the graphite spectrum shown in Fig. 2a and the residual C 1s background pattern in the K 2p hologram. The direction of the forward focusing peak (FFP) and the diffraction ring indicated by white marks in the K 2p hologram correspond to the directions of the nearest neighbouring C atom above. The blue arcs are attributed to the 2×2 -ordered K atomic arrangement, as discussed below.

3D structure images of $(Ca, K)C_8$. The atomic images reconstructed from the C 1s and K 2p photoelectron holograms are summarized in Fig. 3 (Supplementary information Fig.S4). The holography transformation algorithm SPEA-MEM was applied to the photoelectron holograms, and the 3D structure images around the photoelectron emitter C and K atoms were obtained. For the reconstruction from the C 1s hologram, the C atom potential was used for the scatterer, whereas for the K 2p hologram, the K atom potential was used. Therefore, the interatomic distances from the C atom to the K atom and from the K atom to the C atom were underestimated and overestimated, respectively. Figure 3a shows the atomic arrangements reconstructed from the C 1s photoelectron hologram. The cross section at the layer including the photoelectron emitter C atom is indicated. The emitter atom is marked by the ‘x’ in the centre because it does not appear in the reconstructed image. We introduced a translational symmetry mixing operation and examined the reconstructed image by varying the in-plane lattice constant. An in-plane lattice constant of 2.50 ± 0.05 Å resulted in the best converged atomic images. Figure 3b–d were also reconstructed from the C 1s photoelectron hologram but for the layers above the emitter atom by 2.3, 3.3, and 5.7 Å, respectively. Note that the atomic image contrast at each triangular lattice point was different. The first and second neighbouring atom images around the centre appeared as dark and bright spots, respectively, in Fig. 3a, whereas the second neighbouring atom images appeared as bright spots in Fig. 3c. Furthermore, the bright atomic images formed hexagonal and triangular lattices in Fig. 3b,d.

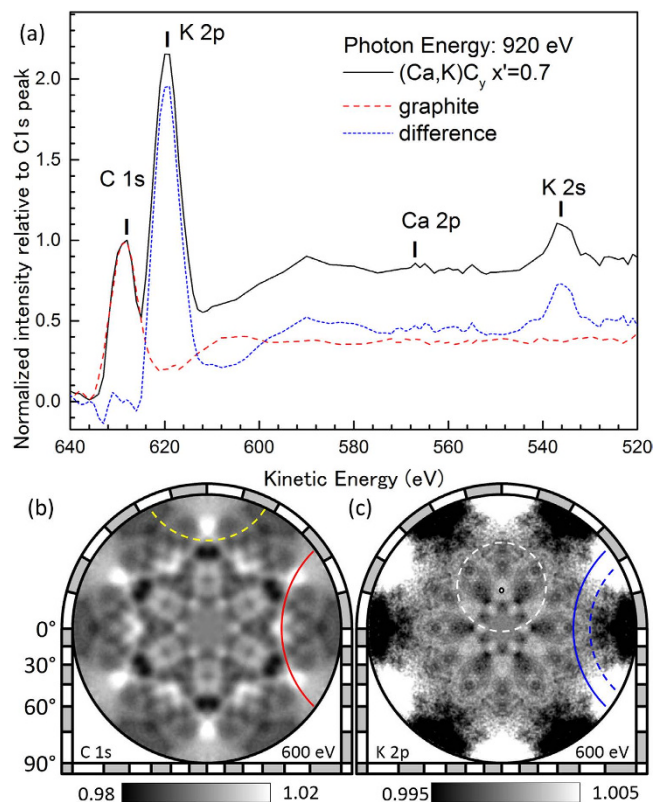


Figure 2. (a) X-ray photoelectron spectra. The K 2*p* core-level spectrum was obtained by subtracting the graphite spectrum from that of $\text{Ca}_{0.7}\text{K}_{0.3}\text{C}_y$. (b) C 1*s* photoelectron intensity angular distribution (hologram). (c) Same as 1b but for K 2*p*.

There are various types of graphene layer stacking, as shown in Fig. 4. The “B” layer can be stacked on the “A” layer with a translational shift equal to the CC bond length in the CC bond direction as shown in Fig. 4b, or the “B” layer can be stacked with a translational shift in the opposite direction, as shown in Fig. 4c. The stacking registry can be determined from the modulation of the atomic image contrast as shown in Fig. 4d–g. For the layer stacked in the AA (Fig. 4d) and AB + AB’ (Fig. 4g) sequences, bright spots form triangular and hexagonal lattices, respectively. The contrast modulation of the C layer at $z_C = 3.3 \text{ \AA}$ (Fig. 3c) is a strong indication that the graphite structure is stacked in the AB pattern. Since the intensity in the blue/red circle in Fig. 3d was smaller than in the white circle, we concluded that atomic arrangement at the C layer at 5.7 \AA is not AB type. Although the first neighbouring atoms were not well reproduced, the photoelectron diffraction simulation analysis described in the next section fitted well, the C layer at 5.7 \AA (Fig. 3d) is attributed to a graphene layer stacked in the AA pattern.

The atomic images in Fig. 3b are located at the centre of C hexagon rings. These spots are attributed to the intercalated K atoms between two AA-stacked graphene layers. The metal–graphene interlayer distance in bulk KC_8 crystals is 2.68 \AA . The underestimation of the K layer height as 2.3 \AA was because of the C atom potential used for the holographic reconstruction¹⁷. Figure 3e is the atomic arrangement at the layer including the photoelectron emitter K atom reconstructed from the K 2*p* photoelectron hologram. For the K atomic image reconstruction, we examined various periodic structure such as 1×1 , $\sqrt{3} \times \sqrt{3}$ and incommensurate lattices. As a result, we found that the 2×2 translational symmetry gave the best converged atomic images. K atoms arranged in 2×2 periodicity were imaged.

C atom sites in the graphene layer have a mirror symmetric relation and they are identical in terms of energy. Therefore, C 1*s* XPS peak for those two sites appear at the same binding energy and cannot be separated using chemical shift information. To separate the two different crystal lattice images from those two types of C atom sites superimposed in the reconstructed images, we defined the following filter patterns $F_+(\mathbf{r})$ and $F_-(\mathbf{r})$. Sum of F_+ and F_- is unity.

$$\mathbf{F}_{\pm} = (1 \pm S_1 S_2 S_3)/2, \quad (1)$$

$$S_i = \sin(\mathbf{a}_i^* \cdot \mathbf{r}/2)/\sin(\pi/3) \quad (2)$$

Figure 5a,b shows the image of the filter pattern $F_+(\mathbf{r})$ and $F_-(\mathbf{r})$, respectively. \mathbf{a}_i^* is a reciprocal lattice vector, as indicated in the inset of Fig. 5a. The triangular lattice point corresponding to the C atom site has a value of 0, 0.5, or 1. By multiplying the filter patterns by the images shown in Fig. 3a,b, we obtained two different lattice images shown coloured in blue (F_+) and red (F_-) in Fig. 5c,d, respectively. The atomic images at the overlapping

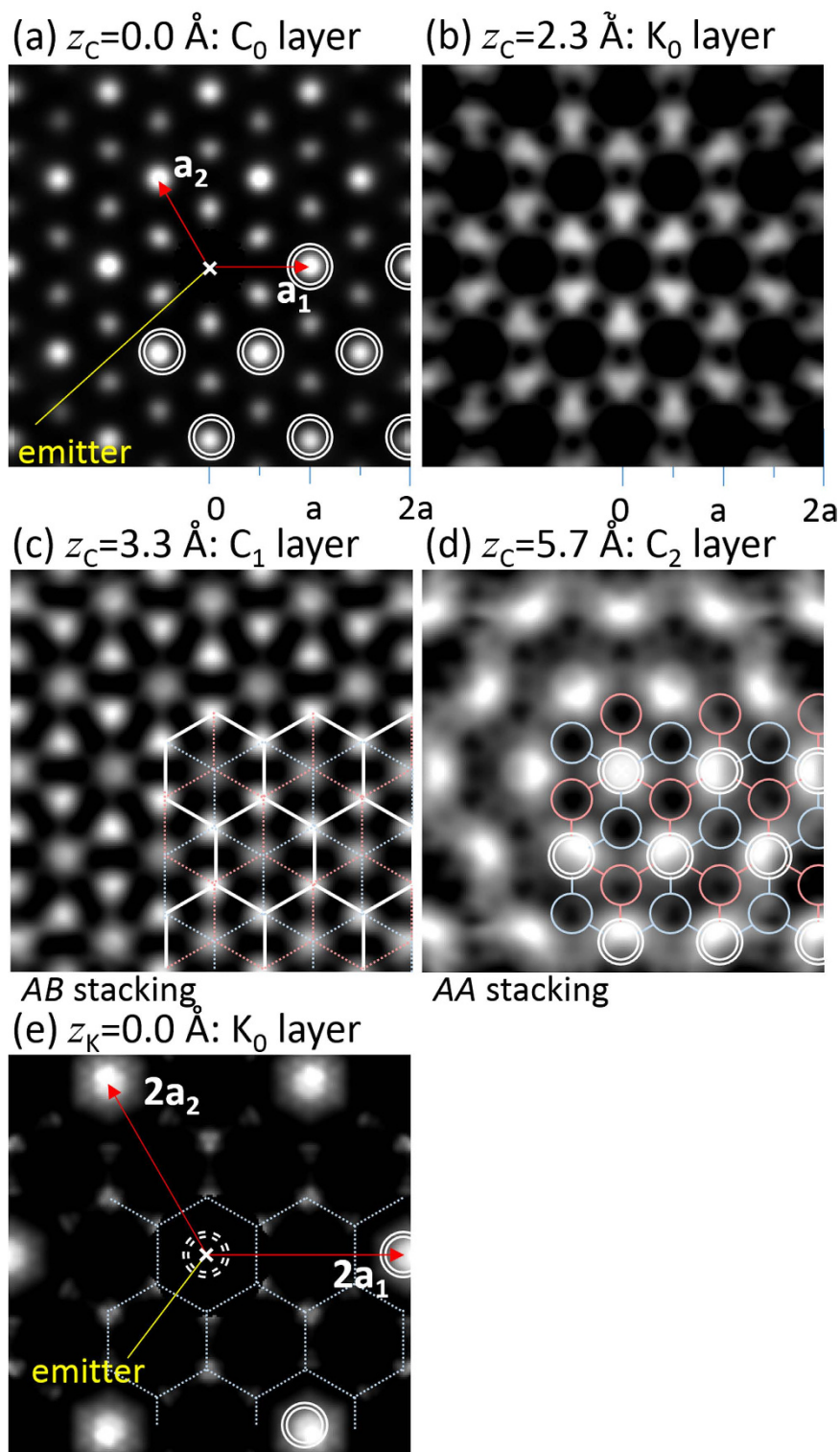


Figure 3. (a) Atomic arrangement reconstructed from the C 1s photoelectron hologram. The cross section at the layer including the photoelectron emitter C atom is indicated. (b–d) Same as 1a but for the layers above the emitter atom by 2.3, 3.3, and 5.7 Å, respectively. (e) Same as 1a but from the K 2p photoelectron hologram.

sites appeared as white spots. Note that in Fig. 5c we obtained a hexagonal lattice, while in Fig. 3e, we obtained K 2×2 lattice. This is because the K lattice in Fig. 5c is seen from the different kind of C emitter atoms, while in Fig. 3e, the emitter is single kind of K atom. By combining one type of lattice image of the C and K layers, we finally obtained the GIC atomic arrangement image shown in Fig. 5e.

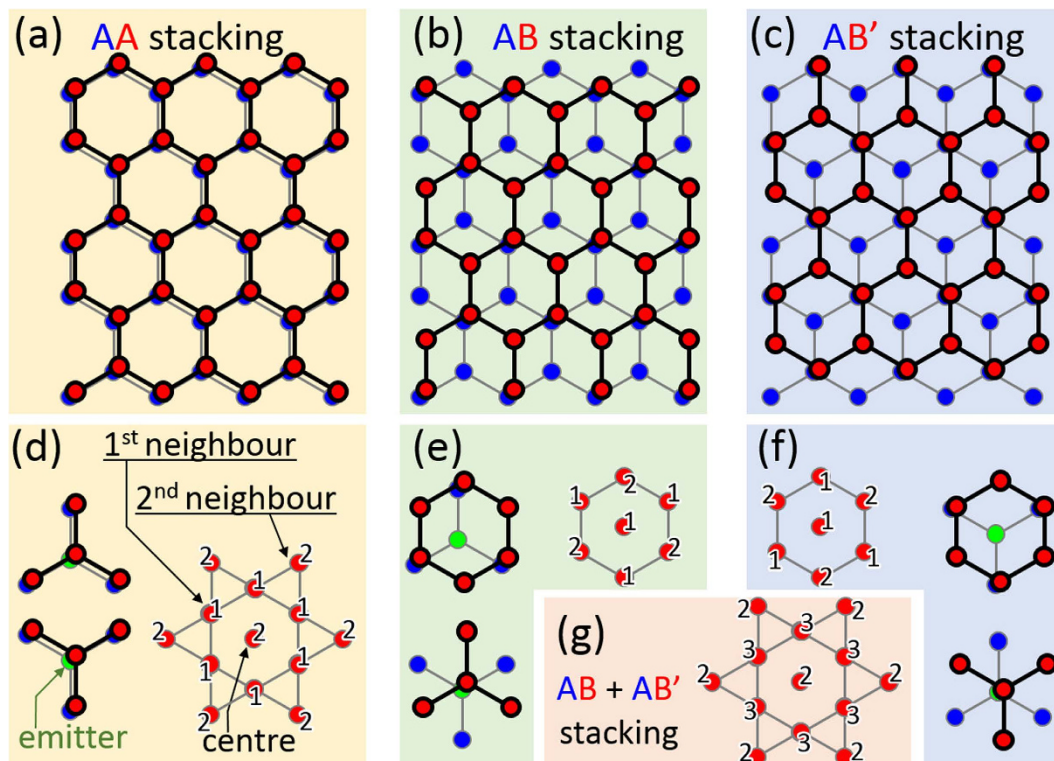


Figure 4. Atomic configuration models of (a) AA, (b) AB, and (c) AB' bilayer stacking structures. Graphene clusters can be stacked on top of the A graphene layer in three different ways. (f–g) The schematic structure model in each stacking geometry and the expected signal intensity ratio at the centre; the first- and the second-neighbouring atoms in the reconstructed real space images.

Local structure evaluation by theoretical approaches. The detailed local structure around the intercalant atoms was revealed as summarized in Fig. 6a,b. The error bars for the interlayer distances for AB and AA stacking were determined from the distribution of vertical atomic images reconstructed by the holography algorithm. We also performed density functional theory (DFT) calculations. Table 1 summarizes the bulk lattice constants^{3,31} and the present data for the cleaved surface compared with the values derived from the DFT calculation. As seen in Table 1, by employing recently proposed van der Waals density functional by Hamada, rev-vdW-DF2³² along with Wu and Gygi's separable form of the vdW kernel^{33,34}, the in-plane as well as inter-layer lattice constants of graphite and bulk KC₈ can be very well reproduced. Note that the in-plane and interlayer lattice parameters are larger than those of graphite and bulk KC₈. The former is attributed to the charge transfer from a metal intercalant atom to the graphite lattice; this is supported by the calculated value. The surface interlayer lattice expansion is attributed to the surface relaxation effect. Although the present experimental value derived from photoelectron holography and the calculated value were within the error, the slight difference between these two values could relate to the effects of excess K and oxygen contamination on the surface.

Based on these structural parameters obtained by photoelectron holography, we simulated C 1s holograms *Q* for the KC₈ and graphite surfaces as shown in Fig. 7b. Using these two simulated holograms as a basis set, the measured C 1s hologram *P* (Fig. 7a) was fitted. Figure 7c shows the root-mean-squared deviations of the measured and simulated C 1s holograms averaged over all pixels and normalized by the diffraction contrast. The linear combination pattern of Q^{KC_8} and Q^{graphite} at a ratio of 42% to 58% most resembled *P* with the lowest root-mean-square deviation. Thus, indicates K intercalation occurs at stage 2. These results also support the conclusion that the cleavage takes place selectively at the layers without Ca atoms and at stage 2-type regions where the graphite layers are weakly bounded.

Discussion

The most important result from the present study is that the cleaved surface does not always represent the averaged bulk structure. The structure and composition of the surface and the bulk can be substantially different, especially in a layered system. Special attention must be paid when using surface-sensitive methods, such as photoelectron spectroscopy and scanning probe microscopy. The structure of the cleaved surface region of GIC was successfully clarified by photoelectron holography and was found to differ substantially from the expected bulk (Ca, K)C₈ crystal structure determined by XRD. These observations revealed that the cleavage preferentially occurred at the KC₈ layers containing no Ca atoms. The K atoms were found to be located in the centre of C hexagons of the graphene sheets stacked in the AA arrangement with an interlayer spacing of 5.7 Å. In addition, the graphite-layered structure was confirmed to exhibit AB stacking and an interlayer spacing of 3.3 Å. This result supports the existence of stage 2-type graphite layers without intercalated metal atoms and the conclusion that

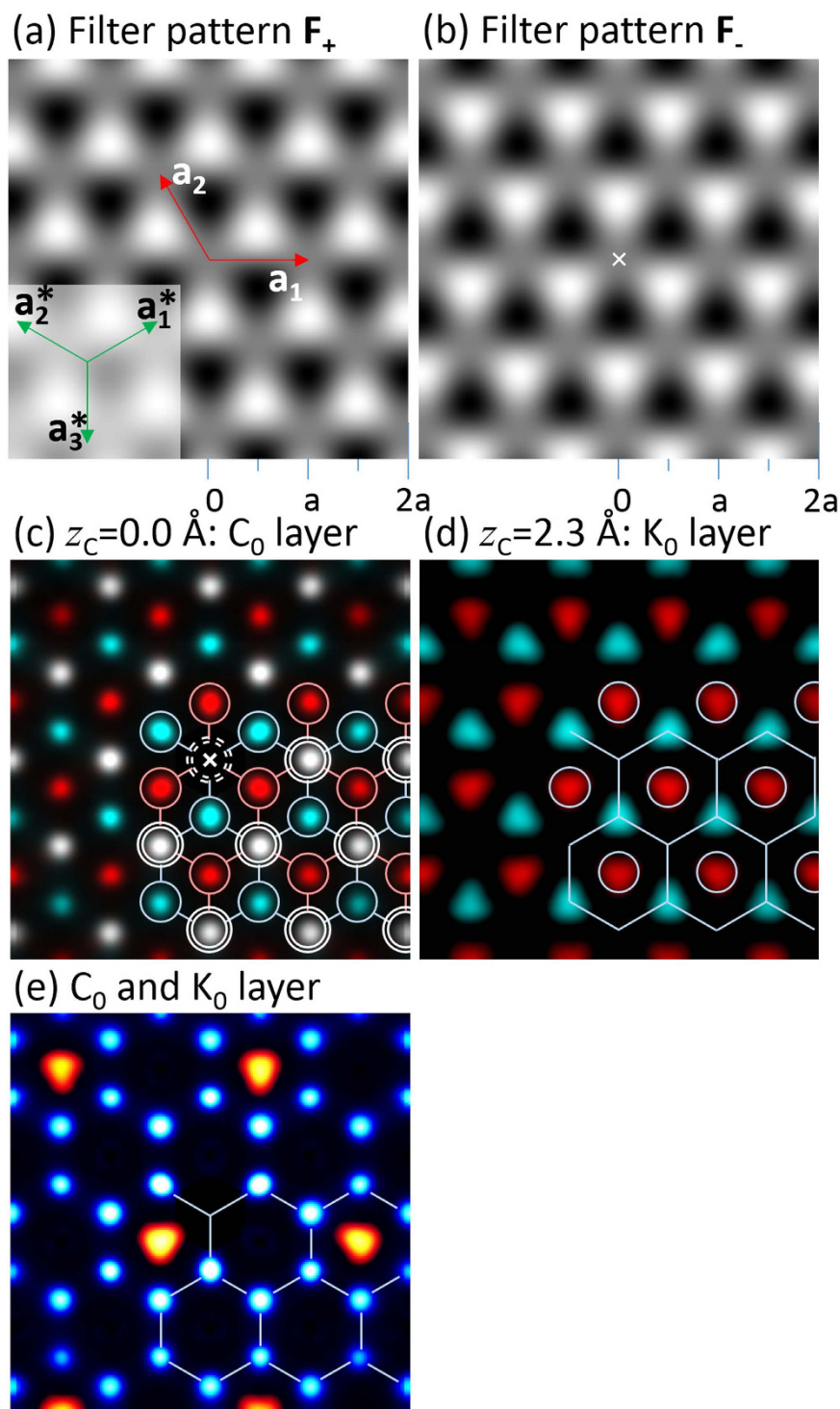


Figure 5. (a,b) Filter patterns. See the text for the definition. (c,d) C and K atom images coloured differently for two different lattices obtained by multiplying images Fig. 3a,b, respectively, with the filter pattern shown in 5a,b. (e) Atomic arrangement image of C and K layers obtained from same type of lattice images for C and K in 5c,d.

cleavage occurs selectively at the weakly bounded layers. Photoelectron holography is a unique method for the 3D visualization of local atomic structures at the surface region.

From the out-of-plane XRD analysis, the graphene interlayer distance was determined to be similar to that of KC_8 , suggesting that the K atoms, which have a larger ion radius, play dominant roles in determining the vertical structure. However, EDX measurements revealed that Ca atoms efficiently contribute to the realization of relatively high T_c despite the low Ca concentration. The observation of the K dominant structure at the cleaved surface implies that Ca atoms are dispersed in the bulk and likely form high T_c domains.

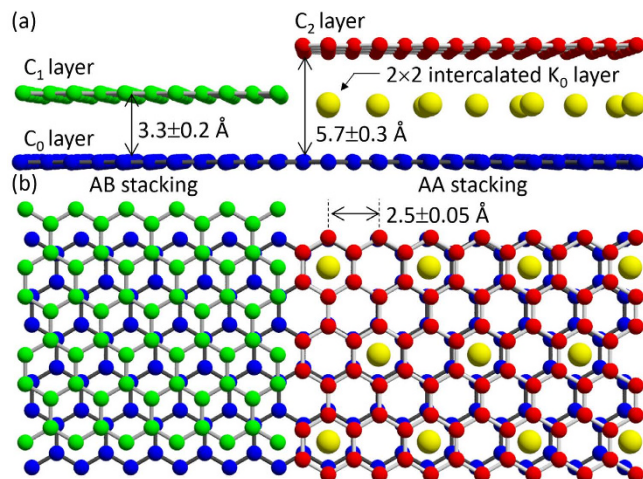


Figure 6. Schematic diagrams of (a) the vertical cross section and (b) top view of GIC.

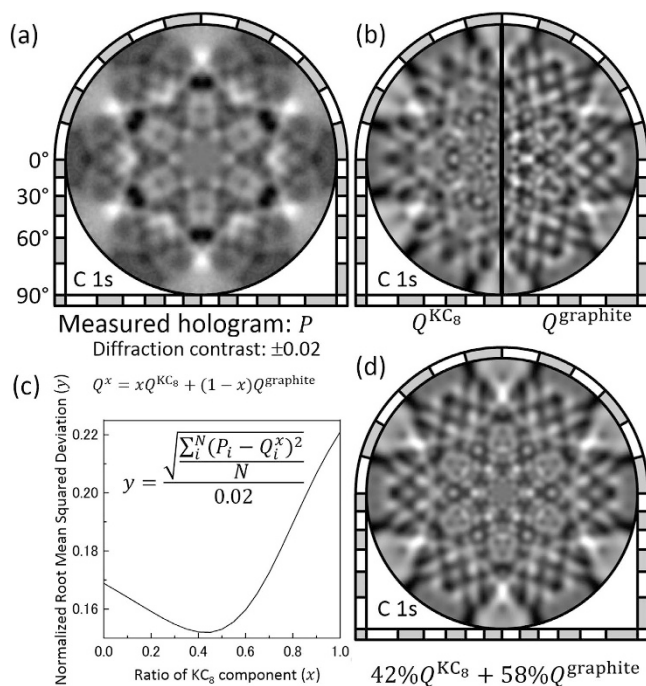


Figure 7. (a) Measured C 1s photoelectron hologram P . (b) Simulated C 1s photoelectron holograms Q^{KC_8} and $Q^{graphite}$ for KC_8 and graphite, respectively. (c) Root-mean-squared deviation of the measured and simulated C 1s holograms averaged over N pixels and normalized by the diffraction contrast of P . (d) Linear combination of the two holograms Q^{KC_8} and $Q^{graphite}$ with a ratio of 42% to 58%.

		bulk (Å)		surface (Å)		
		XRD*	calc.	calc.	Exp. This report	
Graphite	a	2.456	2.456 (0.0%)			1×1
	d_{AA}	3.348	3.356 (+0.2%)	3.348	-0.2%	3.3 ± 0.2 $C_0 - C_1$
KC_8	a	4.96	4.974 (+0.3%)			5.0 ± 0.1 2×2
	d_{AA}	5.35	5.362 (+0.2%)	5.366	+0.1%	5.7 ± 0.3 $C_0 - C_2$

Table 1. Experimental and DFT calculation results for the estimation of the in-plane lattice constant a and the interlayer distances d_{AA} . *Values from reference [31] for graphite and [3] for KC_8 .

Methods

Sample preparation and characterizations. The samples of $(\text{Ca}, \text{K})\text{C}_8$ were prepared using the LMA method⁶. The stoichiometric ratio of Ca and K was established with an excess amount of Li in the vessel, which was heated at 573 K. The Ca/K/Li alloy melted at 573 K. The kish graphite was immersed into the melted Ca/K/Li alloy in the vessel for one week. The superconductivity of the $(\text{Ca}, \text{K})\text{C}_8$ sample was checked by recording the DC magnetic susceptibility (M/H) with a SQUID magnetometer (Quantum Design MPMS2). The XRD pattern of the sample was measured at 297 K using an XRD instrument (Rigaku, Smart Lab-Pro) with a Cu $K\alpha$ source ($\lambda = 1.5418 \text{ \AA}$).

Measurements of photoelectron spectra and holograms. The C 1s and K 2p photoelectron intensity angular distributions (holograms) from the GIC cleaved surface were measured using a display-type spherical mirror analyser (DIANA)^{35,36} at the circularly polarized soft x-ray beamline BL25SU of SPring-8, Japan³⁷. The acceptance solid angle of the analyser was 1π steradian ($\pm 60^\circ$). The x-ray incident direction was set along the surface normal axis. The energy of the electrons emitted from the sample was analysed, and their angular distributions were projected onto the fluorescent screen. A full-hemispherical photoelectron hologram was obtained by rotating the sample azimuthal angle by 360° . We measured for several samples (typically $3 \times 2 \text{ mm}^2$ in size). We surveyed the spatial distribution of the sample and confirmed that when the target area ($1 \times 1 \text{ mm}^2$) were larger than the beam size (diameter: several $10 \mu\text{m}$) were uniform, we get clear diffraction patterns. The holography transformation code SPEA-MEM was used for the real-space atomic arrangement image reconstruction. One-dimensional polar angle photoelectron intensity profiles $I_{\theta,\phi}(\theta_{\text{scan}})$ were derived for every direction, (θ, ϕ) , from the measured holograms. Oscillatory structures resulting from the diffraction rings appeared in the neighbouring atom directions but not in the other directions where no atoms existed. We then calculated the scattering pattern matrix at a kinetic energy of 600 eV. One scattering pattern matrix consisted of a set of fundamental diffraction patterns for polar angles θ_{scan} of 0 to 180° and atomic distances of 0.1 to 1.1 nm. One-dimensional profiles $I_{\theta,\phi}(\theta_{\text{scan}})$ were fitted using the maximum entropy method with these fundamental diffraction patterns corresponding to the positions of 10-pm cubic voxels within 0.7 nm of the emitter atom.

Calculation details. DFT simulations were conducted using the Simulation Tool for Atom TEchnology (STATE-Senri) code. A recently proposed van der Waals density functional by Hamada, rev-vdW-DF2³² was implemented with Wu and Gygi's separable form of the vdW kernel^{33,34}. The inner electrons were replaced by ultrasoft-pseudopotentials and a plane wave basis set with cutoff energies of 36 Ry for wave functions and 400 Ry for charge density is employed. Methfessel and Paxton scheme of the Fermi-level smearing ($\sigma = 0.054 \text{ eV}$) was used to improve the convergence.

References

- Hannay, N. B. *et al.* Superconductivity in graphite compounds. *Phys. Rev. Lett.* **14**, 225–226 (1965).
- Koike, Y., Tanuma, S.-I., Suematsu, H. & Higuchi, K. Superconductivity in the graphite-potassium intercalation compound C_8K . *J. Phys. Chem. Solids* **41**, 1111–1118 (1980).
- Hérol, A., Billaud, D., Guérard, D., Lagrange, L. & Makrini, M. Intercalation of metals and alloys into graphite. *Physica B* **105**, 253–260 (1981).
- Kobayashi, M. *et al.* Superconductivity in the first stage rubidium graphite intercalation compound C_8Rb . *Synthetic Metals* **12**, 341–346 (1985).
- Kim, J. S., Boeri, L., O'Brien, J. R., Razavi, F. S. & Kremer, R. K. Superconductivity in heavy alkaline-earth intercalated graphites. *Phys. Rev. Lett.* **99**, 027001 (2007).
- Emery, N. *et al.* Superconductivity of bulk CaC_6 . *Phys. Rev. Lett.* **95**, 087003 (2005).
- Weller, T. E., Ellerby, M., Saxena, S. S., Smith, R. P. & Skipper, N. T. Superconductivity in the intercalated graphite compounds C_6Yb and C_6Ca . *Nat. Phys.* **1**, 39–41 (2005).
- Okazaki, H. *et al.* Spectroscopic evidence of the existence of substantial Ca 3d derived states the Fermi level in the Ca-intercalated graphite superconductor CaC_6 . *Phys. Rev. B* **80**, 035420 (2009).
- Gauzzi, A. *et al.* Enhancement of superconductivity and evidence of structural instability in intercalated graphite CaC_6 under high pressure. *Phys. Rev. Lett.* **98**, 067002 (2007).
- Kim, J. S., Boeri, L., Kremer, R. K. & Razavi, F. S. Effect of pressure on superconducting Ca-intercalated graphite CaC_6 . *Phys. Rev. B* **74**, 214513 (2006).
- Smith, R. P. *et al.* Pressure dependence of the superconducting transition temperature in C_6Yb and C_6Ca . *Phys. Rev. B* **74**, 024505 (2006).
- DeLong, L. E. *et al.* Observation of anomalies in the pressure dependence of the superconducting transition temperature of potassium-based graphite intercalation compounds. *Phys. Rev. B* **26**, 6315–6318 (1982).
- Heguri, S. *et al.* Superconductivity in the graphite intercalation compound BaC_6 . *Phys. Rev. Lett.* **114**, 247201 (2015).
- Nguyen, H. L. T. *et al.* Fabrication of new superconducting materials, $\text{Ca}_x\text{K}_{1-x}\text{C}_y$ ($0 < x < 1$). *Carbon* **100**, 641–646 (2016).
- Matsushita, T., Guo, F. Z., Matsui, F., Kato, Y. & Daimon, H. Three-dimensional atomic-arrangement reconstruction from an Auger-electron hologram. *Phys. Rev. B* **75**, 085419 (2007).
- Matsushita, T., Matsui, F., Daimon, H. & Hayashi, K. Photoelectron holography with improved image reconstruction. *J. Electron Spectrosc. Relat. Phenom.* **178–179**, 195–220 (2010).
- Matsushita, T., Matsui, F., Goto, K., Matsushita, T. & Daimon, H. Element Assignment for Three-Dimensional Atomic Imaging by Photoelectron Holography. *J. Phys. Soc. Jpn.* **82**, 114005 (2013).
- Matsushita, T. & Matsui, F. Features of Atomic images reconstructed from photoelectron, Auger electron, and internal detector electron holography using SPEA-MEM. *J. Electron Spectrosc. Relat. Phenom.* **195**, 365–374 (2014).
- Kato, Y. *et al.* Dopant-site effect in superconducting diamond (111) studied by atomic stereophotography. *Appl. Phys. Lett.* **91**, 251914 (2007).
- Matsui, F. *et al.* Atomic-Layer Resolved Magnetic and Electronic Structure Analysis of Ni Thin Film on a Cu (001) Surface by Diffraction Spectroscopy. *Phys. Rev. Lett.* **100**, 207201 (2008).
- Matsui, F. *et al.* Selective Detection of Angular-Momentum-Polarized Auger Electrons by Atomic Stereography. *Phys. Rev. Lett.* **114**, 015501 (2015).
- Lühr, T., Winkelmann, A., Nolze, G., Krull, D. & Westphas, C. *Direct Atom Imaging by Chemical-Sensitive Holography Nanoletters* **16**, 3195 (2016)

23. Aizawa, T., Souda, R., Otani, S., Ishizawa, Y. & Oshima, C. Bond softening in monolayer graphite formed on transition-metal carbide surfaces. *Phys. Rev. B* **42**, 11469 (1990).
24. Uchihashi, T., Mishra, P., Aono, M. & Nakamura, T. Macroscopic Superconducting Current through a Silicon Surface Reconstruction with Indium Adatoms: Si(111) - ($\sqrt{7} \times \sqrt{3}$)-In. *Phys. Rev. Lett.* **107**, 207001 (2011).
25. Zhang, T. *et al.* Superconductivity in one-atomic-layer metal films grown on Si(111). *Nature Physics* **6**, 104–108 (2010).
26. Ge, J.-F. *et al.* Superconductivity above 100 K in single-layer FeSe films on doped SrTiO₃. *Nature Materials* **14**, 285–289 (2015).
27. Tegze, M. & Faigel, G. X-ray holography with atomic resolution. *Nature* **380**, 49–51 (1996).
28. Hayashi, K., Happo, N. & Hosokawa, S. Applications of X-ray fluorescence holography to determine local lattice distortions. *J. Electron Spectroscopy and Related Phenomena* **195**, 337–345 (2014).
29. Matsui, F., Matsushita, T. & Daimon, H. Photoelectron Diffraction and Holographic Reconstruction of Graphite. *J. Phys. Soc. Jpn.* **81**, 114604 (2012).
30. Matsui, F. *et al.* Negative Photoelectron Diffraction Replica in Secondary Electron Angular Distribution. *J. Phys. Soc. Jpn.* **81**, 013601 (2012).
31. Sands, D. *Introduction to Crystallography* (Benjamin-Cummings, Reading, Mass., 1969).
32. Hamada I. van der Waals density functional made accurate. *Phys. Rev. B* **89**, 121103 (2014).
33. Wu, J. & Gygi, F. A simplified implementation of van der Waals density functionals for first-principles molecular dynamics applications. *J. Chem. Phys.* **136**, 224107 (2012).
34. Hamamoto, Y., Hamada, I., Inagaki, K. & Morikawa, Y. Self-consistent van der Waals density functionals study of enzene adsorption on Si(100). *Phys. Rev. B* **93**, 245440 (2016).
35. Daimon, H. New display-type analyzer for the energy and the angular distribution of charged particles. *Rev. Sci. Instrum.* **59**, 545 (1988).
36. Matsui, F., Matsushita, T. & Daimon, H. Photoelectron structure factor and diffraction spectroscopy. *J. Electron Spectrosc. Relat. Phenom.* **195**, 347–360 (2014).
37. Saitoh, Y., Kimura, H., Suzuki, Y., Nakatani, T., Matsushita, T., Muro, T., Miyahara, T., Fujisawa, M., Soda, K., Ueda, S., Harada, H., Kotsugi, M., Sekiyama, A. & Suga, S. Performance of a very high resolution soft x-ray beamline BL25SU with a twin-helical undulator at SPring-8. *Rev. Sci. Instrum.* **71**, 3254 (2000).

Acknowledgements

This study was partly supported by Grants-in-Aid (22244045, 24654105, 25287075, 26105004, 26105007, and 26105010) from MEXT and by the Program for Promoting the Enhancement of Research Universities. The photoelectron holography measurements at SPring-8 were supported by 2015A0124 and 2015B1007. K.P. thanks the EPSRC for providing support (EP/K027255). Y.K. is grateful for the support from the LEMSUPER project (JST-EU Superconductor Project) of the Japan Science and Technology Agency (JST) and the ACT-C project of Japan. I. H. acknowledges the financial support from MEXT through the “World Premier International Research Center Initiative (WPI),” and the “Development of Environmental Technology using Nanotechnology” program.

Author Contributions

F.M. and Y.K. designed this research project and supervised the experiments. R.E., S.N., M.I., E.U. and H.G. synthesized and characterized the (Ca, K)C₈ samples. R.E., S.N., M.I., E.U. and H.G. performed the resistance measurements. F.M., R.E., S.N., E.U., K.S. and H.D. measured the photoelectron spectra and holograms. F.M. and T.M. performed the holography reconstruction calculations. Y.H., I.H. and Y.M. conducted the DFT calculations. F.M. and Y.K. discussed the experimental results with T.M. during this study. F.M. and Y.K. managed (edited) all parts of the paper.

Additional Information

Supplementary information accompanies this paper at <http://www.nature.com/srep>

Competing financial interests: The authors declare no competing financial interests.

How to cite this article: Matsui, F. *et al.* Photoelectron Holographic Atomic Arrangement Imaging of Cleaved Bimetal-intercalated Graphite Superconductor Surface. *Sci. Rep.* **6**, 36258; doi: 10.1038/srep36258 (2016).

Publisher's note: Springer Nature remains neutral with regard to jurisdictional claims in published maps and institutional affiliations.



This work is licensed under a Creative Commons Attribution 4.0 International License. The images or other third party material in this article are included in the article's Creative Commons license, unless indicated otherwise in the credit line; if the material is not included under the Creative Commons license, users will need to obtain permission from the license holder to reproduce the material. To view a copy of this license, visit <http://creativecommons.org/licenses/by/4.0/>

© The Author(s) 2016